DCPT-14/41

Aloof Baby Skyrmions

Petja Salmi and Paul Sutcliffe

Department of Mathematical Sciences, Durham University, Durham DH1 3LE, U.K.

petja.salmi@durham.ac.uk & p.m.sutcliffe@durham.ac.uk

September 2014

arXiv:1409.8176v1 [hep-th] 29 Sep 2014

Abstract

We show that a suitable choice for the potential term in the two-dimensional baby Skyrme model yields solitons that have a short-range repulsion and a long-range attraction. The solitons are therefore aloof, in the sense that static multi-soliton bound states have constituents that preserve their individual identities and are sufficiently far apart that tail interactions yield small binding energies. The static multi-soliton solutions are found to have a cluster structure that is reproduced by a simple binary species particle model. In the standard three-dimensional Skyrme model of nuclei, solitons are too tightly bound and are often too symmetric, due to symmetry enhancement as solitons coalesce to form bound states. The aloof baby Skyrmion results endorse a way to resolve these issues and provides motivation for a detailed study of the related three-dimensional version of the Skyrme model.

1 Introduction

In the standard three-dimensional Skyrme model of nuclei, solitons coalesce to form bound states that are often highly symmetric [1]. However, in comparison to experimental data on nuclei, the solitons are too tightly bound and are often too symmetric. Including massive pions does change the soliton symmetries (for a sufficiently large number of solitons) and produces solutions with a more realistic cluster structure [2], but the solitons are still too tightly bound. One strategy for reducing soliton binding energies is to consider a modified Skyrme model that is a perturbation from a BPS theory, either by including terms in the Lagrangian that are only zero or sixth order in derivatives [3, 4] or by adding a tower of vector mesons to the standard Skyrme model [5].

An alternative approach to a near BPS theory is to consider a family of theories that interpolates between the standard Skyrme model and a theory in which inter-soliton forces are repulsive. Binding energies can then be made suitably small by choosing the value of the interpolation parameter sufficiently close to the repulsive limit. An appropriate repulsive theory in three dimensions has recently been identified and consists of a Skyrme term and a potential term, chosen so that a topological energy bound can be attained only in the one-soliton sector [6]. This makes the above interpolation scheme feasible and work is currently underway to investigate this in detail [7].

The purpose of the current paper is to investigate a lower-dimensional analogue of this scheme, where both numerical and analytic methods are easier to employ. The standard baby Skyrme model [8] is a two-dimensional analogue of the standard Skyrme model. Furthermore, a version of the baby Skyrme model with repulsive solitons has been known for a long time [9], and in fact this has the same potential term as in the recently discovered repulsive Skyrme model [6]. We demonstrate that the interpolating family includes theories where the solitons have a short-range repulsion and a long-range attraction. These solitons are therefore aloof, in the sense that static multi-soliton bound states have constituents that preserve their individual identities and are sufficiently far apart that tail interactions yield small binding energies. The static multi-soliton solutions are found to have a cluster structure that is reproduced by a simple binary species particle model.

The results presented on two-dimensional aloof solitons provides evidence to support the view that similar aloof solitons in three dimensions could address some of the current problematic issues with soliton binding energies and symmetries in the standard Skyrme model. Not only does this work supply additional motivation to study the three-dimensional problem but it also demonstrates the utility of point particle models in predicting the forms and energies of multi-soliton bound states.

2 The aloof baby Skyrme model

The field of the baby Skyrme model is a three-component unit vector $\boldsymbol{\phi} = (\phi_1, \phi_2, \phi_3)$, with associated static energy

$$E = \int \left(\frac{1}{2} \partial_i \boldsymbol{\phi} \cdot \partial_i \boldsymbol{\phi} + \frac{1}{4} (\partial_i \boldsymbol{\phi} \times \partial_j \boldsymbol{\phi}) \cdot (\partial_i \boldsymbol{\phi} \times \partial_j \boldsymbol{\phi}) + V \right) d^2x, \tag{2.1}$$

where $V(\boldsymbol{\phi})$ is a potential and x_i, are coordinates in the plane, with $i = 1, 2$. In the standard baby Skyrme model [8] the potential is taken to be

$$V = m^2(1 - \phi_3), \tag{2.2}$$

which is the analogue of the conventional pion mass term in the Skyrme model [10]. The constant m gives the mass of the fields ϕ_1 and ϕ_2, associated with elementary excitations around the unique vacuum $\boldsymbol{\phi} = (0, 0, 1)$.

Finite energy requires that the field takes the vacuum value at all points at spatial infinity, $\boldsymbol{\phi}(\infty) = (0, 0, 1)$. This compactification means that topologically $\boldsymbol{\phi}$ is a map between two-spheres, with an associated integer winding number $N \in \mathbb{Z} = \pi_2(S^2)$. This topological charge (or soliton number) is the analogue of the baryon number in the Skyrme model and may be calculated as

$$N = -\frac{1}{4\pi} \int \boldsymbol{\phi} \cdot (\partial_1 \boldsymbol{\phi} \times \partial_2 \boldsymbol{\phi}) \, d^2x. \tag{2.3}$$

There is an attractive channel for inter-soliton forces in the standard baby Skyrme model and hence there are multi-soliton bound states that have been investigated numerically in some detail [8, 11]. In particular, the 2-soliton bound state is radially symmetric as there is no short-range repulsion in the attractive channel, so two single solitons coalesce into one radial structure.

Several other choices for the potential have been investigated, but the one of particular relevance to the present paper is the potential introduced in [9]

$$V = m^2(1 - \phi_3)^4. \tag{2.4}$$

The fields ϕ_1 and ϕ_2 are both massless for this choice of potential, so m is simply a parameter of the theory that controls the size of the soliton, rather than a mass. The theory with potential (2.4) has the interesting property that the $N = 1$ soliton can be written down explicitly in closed form, although there are no multi-soliton bound states as there is a repulsive force between solitons [9]. These features are explained by the fact that there is a topological energy bound [12]

$$E \geq 4\pi N \left(1 + \frac{4\sqrt{2}}{3} m \right) \tag{2.5}$$

that is attained only in the $N = 1$ sector, by the 1-soliton solution

$$\boldsymbol{\phi} = \left(\frac{2\lambda x_1}{x_1^2 + x_2^2 + \lambda^2}, \frac{2\lambda x_2}{x_1^2 + x_2^2 + \lambda^2}, \frac{x_1^2 + x_2^2 - \lambda^2}{x_1^2 + x_2^2 + \lambda^2} \right), \tag{2.6}$$

where $\lambda = 1/(2^{1/4}\sqrt{m})$ is the width of the soliton. With the repulsive potential (2.4) this is the exact 1-soliton solution positioned at the origin $(x_1, x_2) = (0, 0)$, where $\boldsymbol{\phi} = (0, 0, -1)$, but the position can be moved to an arbitrary point in the plane by making use of the translational symmetry of the theory. An arbitrary phase can also be introduced into the solution by acting with the global $U(1)$ symmetry that rotates the first two components of $\boldsymbol{\phi}$.

Given the potentials (2.2) and (2.4), that produce an attractive and repulsive force between solitons respectively, we can now implement the strategy described in the introduction and consider a potential that is a linear combination of the two, with the aim of generating a short-range repulsion and a long-range attraction that combine to yield weakly bound multi-solitons. Explicitly, the potential is taken to be

$$V = m^2\bigg(\mu(1-\phi_3) + (1-\mu)(1-\phi_3)^4\bigg), \tag{2.7}$$

where $\mu \in [0, 1]$ is a parameter that interpolates between the repulsive model $\mu = 0$ and the standard baby Skyrme model $\mu = 1$. It will turn out that the choice $\mu = \frac{1}{2}$ is sufficient to achieve our intended aims, so we restrict to this value for most of our investigations and concentrate on the resulting potential

$$V = \frac{m^2}{2}(1-\phi_3)(1+(1-\phi_3)^3). \tag{2.8}$$

The value of the constant m merely determines an overall length scale, with the mass of the elementary excitations equal to $m/\sqrt{2}$. The numerical studies in [8, 11], for the potential (2.2), selected the value $m^2 = 0.1$, so to aid comparison with previous studies we take this same value for m.

3 Soliton solutions

In this section we investigate static soliton solutions of the aloof baby Skyrme model with potential (2.8) and $m^2 = 0.1$. A radially symmetric field with topological charge N is given by

$$\boldsymbol{\phi} = (\sin f \cos(N\theta + \chi), \sin f \sin(N\theta + \chi), \cos f), \tag{3.1}$$

where r and θ are polar coordinates in the plane with $f(r)$ a monotonically decreasing radial profile function such that $f(0) = \pi$ and $f(\infty) = 0$. The constant χ is an internal phase that can be set to zero by applying the global symmetry that rotates the ϕ_1, ϕ_2 components. Although the internal phase is irrelevant in the above radial ansatz, the relative phase between two separated solitons is important and plays a crucial role in the inter-soliton force.

The radial profile function satisfies a second order ordinary differential equation that is easily derived by substituting the radial ansatz (3.1) into the energy (2.1) and performing the variation. A numerical solution for the profile function with $N = 1$ is shown in the left

image in Figure 1 and yields the 1-soliton energy $E_1 = 20.27$. The right image in Figure 1 shows a plot of the function ϕ_3 in the plane, which is a convenient way to display the soliton solutions and will be used from now on.

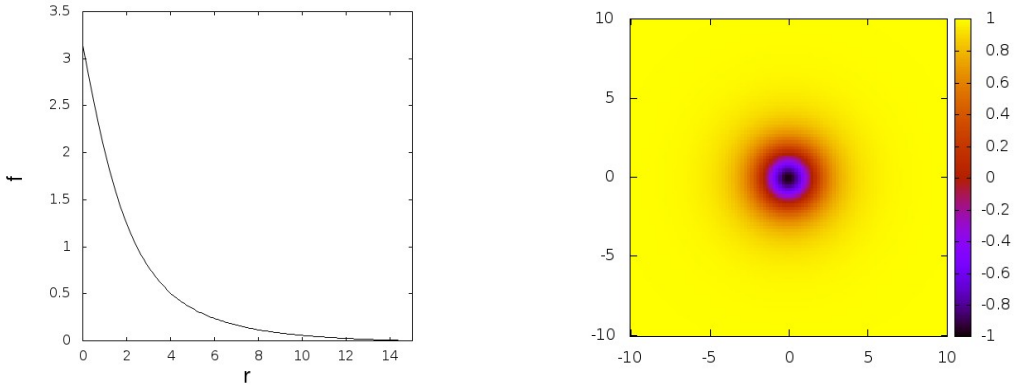

Figure 1: The $N = 1$ soliton. The left image is the profile function $f(r)$ and the right image is a plot of ϕ_3 in the plane.

It turns out that radially symmetric solitons with $N > 1$ are unstable in this theory and we must turn to numerical field theory computations in the plane to study multi-solitons. We apply a field theory energy minimization algorithm using fourth order finite difference approximations for the spatial derivatives on a lattice with 251×251 grid points and a lattice spacing $\Delta x = 0.2$. The field is fixed at the vacuum value $\boldsymbol{\phi} = (0, 0, 1)$ at the boundary of the grid. Note that, for clarity, the full extent of the simulation region is not displayed in the figures that follow. The energy minimization algorithm is an adaptation of the one described in detail in [1], where it is applied to the standard three-dimensional Skyrme model. A range of charge N initial conditions have been used, including perturbations that break the radial symmetry of configurations of the form (3.1), and N well-separated single solitons with random initial positions and phases.

The minimal energy 2-soliton is displayed in the first image of Figure 2, where it can be seen that it resembles two separated single solitons. This 2-soliton has energy $E_2 = 39.84$, which is less than $2E_1$, confirming that it is indeed a bound state. Rather than list the energy E of an N-soliton solution it is more convenient to present the binding energy $\Delta = NE_1 - E$, which is the energy required to split the bound state into N single solitons. The 2-soliton has binding energy $\Delta = 2E_1 - E_2 = 0.70$, which is less than 2% of the total energy, so the solitons are indeed weakly bound in this theory. Although the two solitons form a bound state they keep their individual identities, remaining aloof rather than merging into a radial configuration (which is the situation in the standard baby Skyrme model). For comparison, the energy of the unstable radially symmetric $N = 2$ configuration is $E = 40.49$, which is very close to twice the energy of a single soliton.

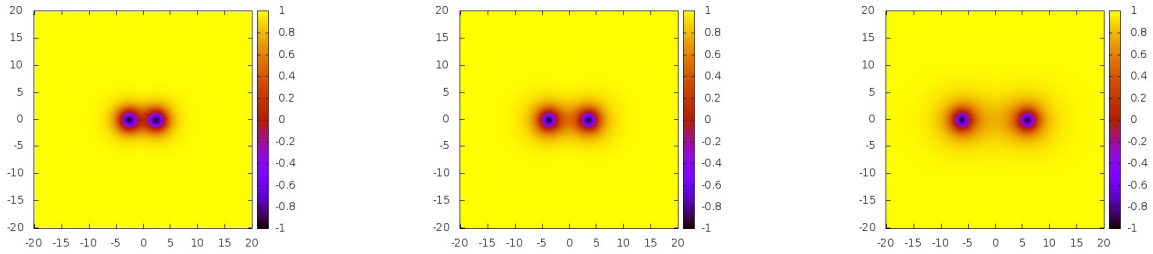

Figure 2: A plot of ϕ_3 for the 2-soliton with $\mu = 0.5$, 0.2, 0.05 (left to right).

As mentioned above, fixing the interpolation parameter value to $\mu = 0.5$ is sufficient to induce the features that we wish to highlight. However, to demonstrate that there is nothing special about this choice we display the 2-soliton solution for the parameter values $\mu = 0.2$ and $\mu = 0.05$. as the second and third images in Figure 2. As expected, as μ decreases towards the repulsive limit $\mu = 0$ the solitons becomes increasingly aloof, with the separation between the constituent solitons increasing and binding energies decreasing. From now on we shall consider only the value $\mu = 0.5$, being aware that the qualitative features should persist for all sufficiently small values of μ.

The static 2-soliton solution suggests that there is a short-range repulsion and a long-range attraction between two single solitons. The long-range attraction can be understood analytically by calculating the asymptotic interaction energy between two well-separated solitons at the linear level. This calculation has been performed for the standard baby Skyrme model [8] and the result can be applied directly to the aloof model with $\mu \in (0, 1]$, because the last term in the potential (2.7) does not contribute to the interaction potential at the linear level. For two solitons with a separation R and a relative phase χ the asymptotic result for the large R interaction energy $U^{\rm asy} \sim E - 2E_1$ is [8]

$$U^{\rm asy}(R, \chi) = C \cos\chi \frac{e^{-m\sqrt{\mu}R}}{\sqrt{R}}, \tag{3.2}$$

where C is a positive constant that depends on m and μ.

This formula shows that two solitons that are in phase ($\chi = 0$) are repulsive, as the interaction energy is positive. The most attractive channel is when the two solitons are exactly out of phase ($\chi = \pi$), so that the interaction energy is maximally negative and there is an attractive force at large separations. The fact that this long-range attractive force turns into a short-range repulsive force cannot be determined by a linear analysis because it is due to the last term in the potential (2.7), which is a nonlinear effect as the linear contribution vanishes [8]. We therefore turn to a numerical computation of the interaction potential.

First we compute the interaction potential, $U_0(R)$, for two solitons with separation R and relative phase $\chi = 0$. An initial condition containing two solitons with given positions and phases can be constructed using a product ansatz as follows. Introduce the Riemann sphere

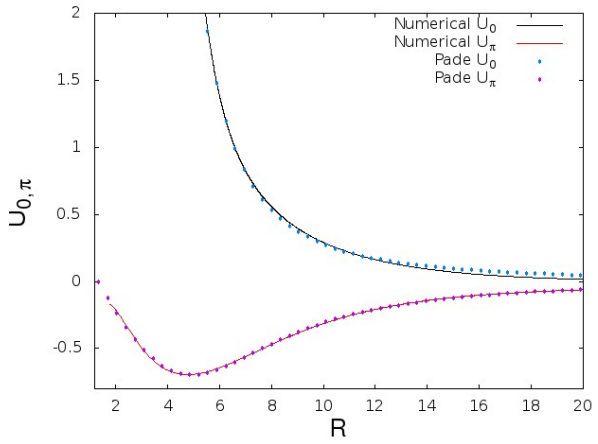

Figure 3: The numerically computed interaction potential U_0 for two solitons that are in phase (upper blue curve) and the interaction potential U_π for two solitons that are out of phase (lower red curve). Dots denote the Padé approximants of order [3/4] described in the text.

coordinate $W = (\phi_1 + i\phi_2)/(1 - \phi_3)$, obtained by stereographic projection of $\boldsymbol{\phi}$. Let W_1 and W_2 be the associated fields of two $N = 1$ solitons, with arbitrary positions and phases, and construct the $N = 2$ field W via

$$W = \frac{W_1 W_2}{W_1 + W_2}, \tag{3.3}$$

which provides $\boldsymbol{\phi}$ by inverse stereographic projection. We take this form of initial condition with relative phase $\chi = 0$ and a range of small initial separations $R_0 \in [3, 5]$, and apply our energy minimization algorithm, computing the separation R and energy E as the minimization takes place. As there is a repulsive force between the solitons, R increases and E decreases, producing the in phase interaction potential $U_0(R) = E - 2E_1$ displayed as the upper black curve in Figure 3. The computed potential $U_0(R)$ is independent of the initial separation R_0 over the range shown, where $R > R_0$.

To compute the interaction potential, $U_\pi(R)$, for two solitons with separation R and relative phase $\chi = \pi$, we use the same product ansatz to compute an initial condition for two out of phase solitons, but this time with a large initial separation R_0. The results presented used the value $R_0 = 20$, but the results are independent of R_0 providing it is sufficiently large. This time, rather than using an energy minimization algorithm, we evolve the full nonlinear, energy conserving, second order time dependent field equations that follow from the relativistic baby Skyrmion Lagrangian associated with the static energy (2.1). As the inter-soliton force is attractive at long-range, the soliton separation R decreases with time. Although the total energy is conserved in relativistic dynamics (and is conserved to a high accuracy in our numerical computations) the static energy E given by (2.1) is not conserved because of the missing kinetic energy contribution. Monitoring the separation R and the static energy E as a function of time results in the plot of the interaction potential

$U_\pi(R) = E - 2E_1$, displayed as the lower red curve in Figure 3.

We have been able to compute the interaction potential using this method by exploiting the fact that baby Skyrmion dynamics produces very little radiation, and binding energies are small hence the soliton speeds remain low. We see from the curve for $U_\pi(R)$ in Figure 3 that the turning point is reproduced at the correct soliton separation and binding energy of the static 2-soliton solution. Furthermore, the short-range repulsion is now evident, and the reason we are able to compute the potential $U_\pi(R)$ almost all the way to $R = 0$ is because the unstable radially symmetric $N = 2$ configuration has an energy very close to twice that of the 1-soliton.

The numerical computations confirm that solitons that are in phase ($\chi = 0$) are repulsive and solitons that are out of phase ($\chi = \pi$) have a long-range attraction and a short-range repulsion. In what follows it will be useful to have an analytic approximation to the interaction potentials $U_\chi(R)$ for these two relative phases $\chi = 0, \pi$. In the range of R of interest (essentially the range displayed in Figure 3), both interaction potentials can be described by a Padé approximant of order [3/4] given by

$$U_\chi(R) = \frac{\sum_{j=0}^{3} a_j R^j}{\sum_{j=0}^{4} b_j R^j}. \tag{3.4}$$

For $\chi = \pi$ we make use of the fact that the energy of the $N = 2$ radial solution is approximately twice the 1-soliton energy to impose the condition $U_\pi(0) = 0$, which fixes the constant $a_0 = 0$, and without loss of generality we set the normalisation by choosing $b_0 = 1$. For $\chi = 0$ we require that $U_0(R)$ diverges as $R \to 0$, hence we fix $b_0 = 0$ and set the normalisation by choosing $a_0 = 1$. The remaining constants can be found in Table 1 and were determined by a least squares fit to the numerical data presented in Figure 3. The dots in Figure 3 show the results of evaluating these Padé approximants and confirm that they provide good approximations to the interaction potentials.

	a_0	a_1	a_2	a_3	b_0	b_1	b_2	b_3	b_4
U_π	0	1.355	-1.024	0.012	1	0.716	1.271	-0.298	0.041
U_0	1	8.469	3.904	-0.019	0	2.583	-0.609	-0.868	0.254

Table 1: The coefficients in the [3/4] Padé approximants of the interaction potentials U_π, U_0.

Turning now to solitons of higher charge, in Figure 4 we present the global minimal energy static N-soliton for $2 \leq N \leq 12$. Most of these solutions were obtained by applying our field theory energy minimization algorithm to initial conditions containing N single solitons with random positions and internal phases. Many local energy minima were also obtained and we shall discuss this aspect further in the following section, together with more details regarding the construction of initial conditions.

The global minima displayed in Figure 4 reveal a range of configuration types including linear chains, circular necklaces, square arrays and cluster structures. The 7-soliton is an interesting example and resembles a soliton analogue of a halo nucleus, with 6 solitons in

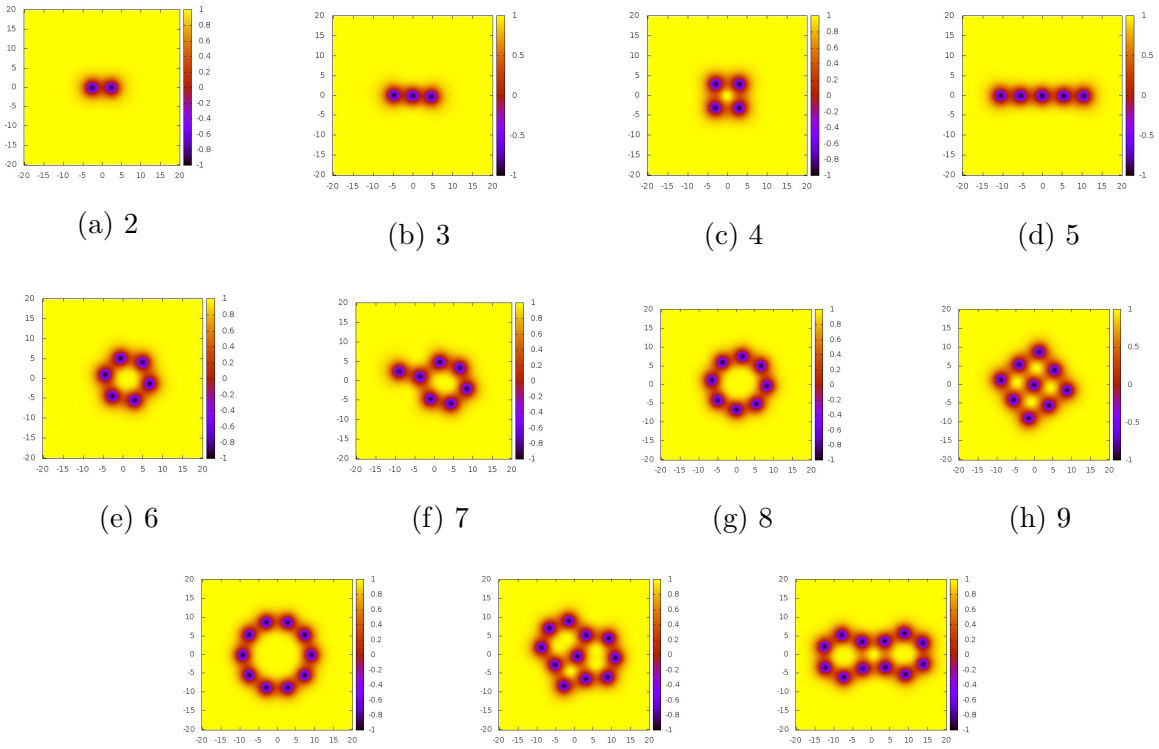

(a) 2 (b) 3 (c) 4 (d) 5

(e) 6 (f) 7 (g) 8 (h) 9

(i) 10 (j) 11 (k) 12

Figure 4: Plots of ϕ_3 for global energy minima for N-solitons with $2 \leq N \leq 12$.

the core and a weakly bound single soliton in the halo. The 12-soliton clearly has a cluster decomposition into two 6-solitons, being reminiscent of the recurrent clustering phenomenon in light nuclei. The fact that the basic building block in our baby Skyrme model appears to be the 6-soliton, compared to the 4-nucleon alpha-particle in nuclei, is likely a result of the two-dimensional nature of our toy model.

In Figure 5 we plot the binding energy per soliton Δ/N for these minimal energy N-soliton solutions (the precise values for Δ will be presented in a later table). The plot displays the correct qualitative features of nuclear binding energies (in the absence of Coulomb effects) with a general increase of the binding energy per nucleon towards a plateau, and tighter binding for even numbers of nucleons in comparison to neighbouring odd numbers.

The variety of pattern types displayed in Figure 4 make it far from obvious to predict the form taken by the minimal energy N-soliton for any given value of N. However, the fact that the constituent single solitons remain aloof means that a point particle model may be able to predict the structures obtained from the field theory computations. In the following section we introduce a binary species point particle model and demonstrate that it indeed provides an excellent approximation and is able to predict the form of all the soliton solutions obtained.

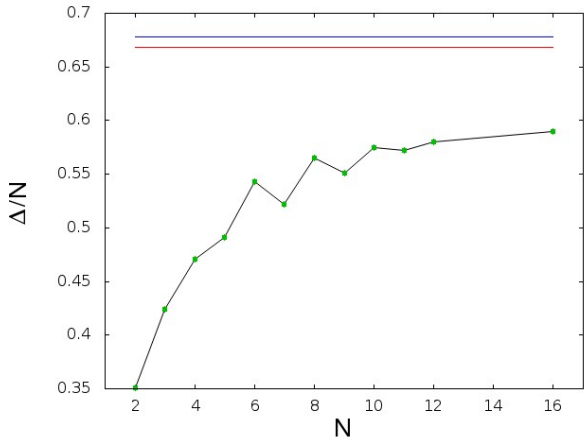

Figure 5: The binding energy per soliton Δ/N. The upper blue and red lines denote the values for the hexagonal and square lattice respectively.

4 A binary species particle model

As we have seen, the attractive channel for two solitons is when the relative phase between the two solitons is equal to π. This suggests that the constituent single solitons in an N-soliton solution can be allocated into two groups, where all solitons in a given group have the same phase and there is a relative phase of π between two solitons in different groups. An appropriate arrangement of the solitons will then allow a large number of attractive channel pairings, with repulsive pairings being suppressed by optimal spatial positioning.

Our point particle model makes this assumption and is a binary species model where we label the two species as blue and red. Blue particles represent single solitons with an internal phase $\chi = 0$ and red particles are solitons with an internal phase $\chi = \pi$. Two particles of different colours are therefore in the attractive channel and we define the potential between them to be given by the Padé approximant (3.4) to the potential $U_\pi(R)$, where R is the distance between the two point particles. Similarly, we define the potential between two particles of the same colour to be the Padé approximant to the potential $U_0(R)$. To create as many attractive pairs as possible we alternately label the particles as blue and red, so that there are $N_{\rm red} = \lfloor N/2 \rfloor$ red particles and $N_{\rm blue} = N - N_{\rm red}$ blue particles. The particle binding energy δ is simply defined to be minus the sum over all pairs of interactions, that is

$$\delta = -\sum_{i=2}^{N} \sum_{j=1}^{i-1} U_{\chi_{ij}}(|\mathbf{x}^{(i)} - \mathbf{x}^{(j)}|), \tag{4.1}$$

where $\mathbf{x}^{(1)}, \ldots, \mathbf{x}^{(N)}$ are the positions of the N particles in the plane and $\chi_{ij} = 0$ if particles with positions $\mathbf{x}^{(i)}$ and $\mathbf{x}^{(j)}$ are of the same colour and $\chi = \pi$ otherwise.

To compute local maxima of the particle binding energy we use a simple multi-start hill climbing algorithm with 1000 starts for each particle number N, where each start consists of N random positions for the particles inside the square $[-20, 20] \times [-20, 20]$. The results for

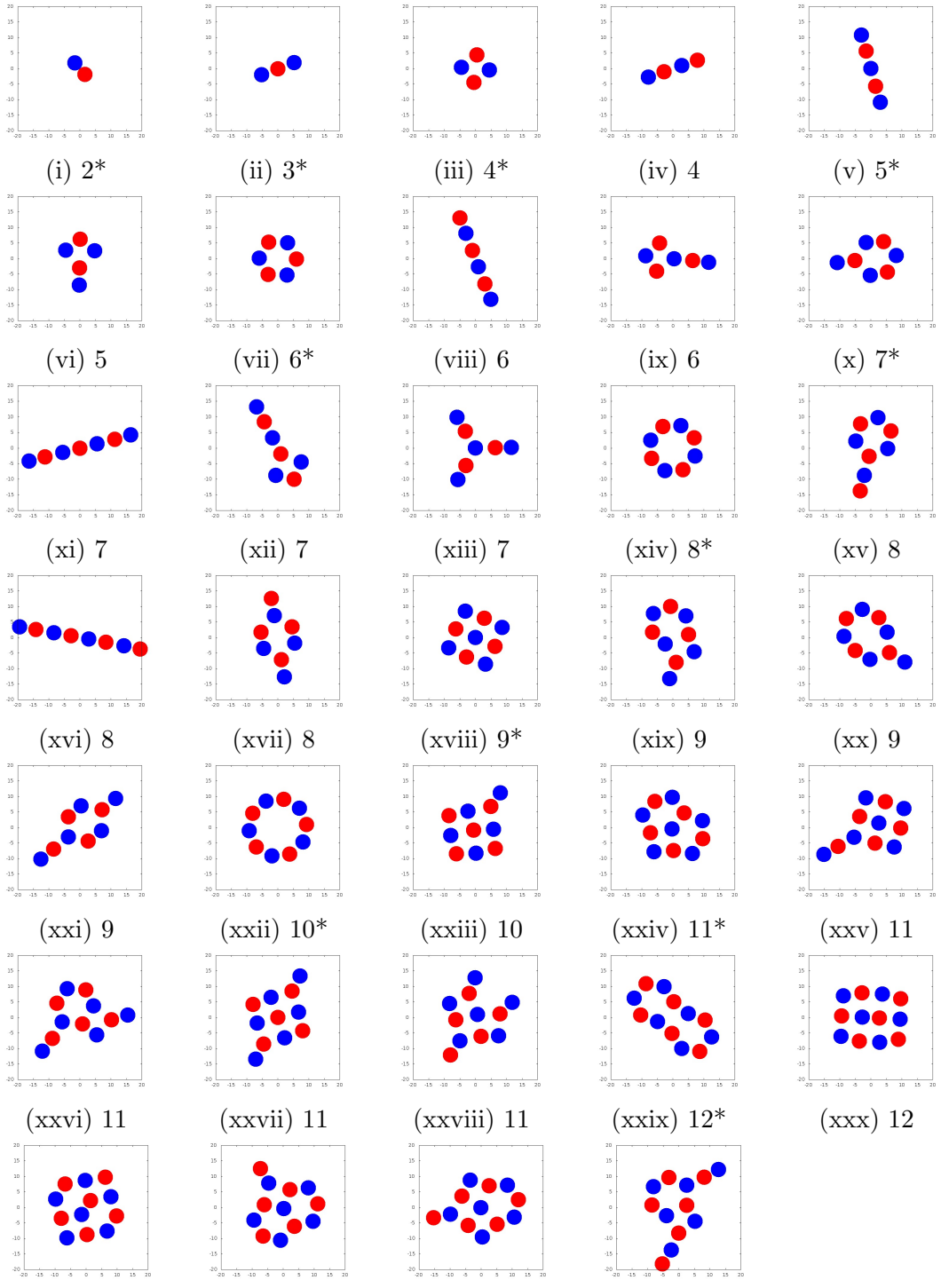

Figure 6: Local maxima of the binding energy δ in the N-particle model with $2 \leq N \leq 12$. * denotes the global maximum of δ for each value of N.

$2 \leq N \leq 12$ are displayed in Figure 6 by plotting blue and red discs, centred at the positions of the blue and red particles, with each disc diameter equal to the value of the separation R at which the out of phase interaction potential, $U_\pi(R)$, is minimized.

A total of 34 local maxima of δ were obtained from these 11000 random starts and all are shown in Figure 6, ordered first by increasing particle number N and then by decreasing particle binding energy δ within solutions with the same value of N. For each N the configuration with the global maximum of δ is denoted by a *, and a comparison of these configurations with the soliton solutions in Figure 4 reveals that the particle model predicts the correct arrangement in each case. Furthermore, all of the local maxima of the particle binding energy have an associated static N-soliton solution that is a local minimum of the field theory energy. These soliton solutions have been obtained by using the particle results to specify the initial positions and phases of the constituent single solitons used to generate initial conditions for the field theory energy minimization algorithm.

For all 34 configurations the value of the particle binding energy δ is listed in Table 2, together with the soliton binding energy Δ of the associated N-soliton solution. The first column in this table denotes the configuration by reference to the labelling in Figure 6. We see from this table that the particle binding energy is a reasonable approximation to the soliton binding energy, although it systematically underestimates the soliton value. More importantly, there is an exact agreement between the particle model binding energy ordering and that of the soliton model. Thus the particle model correctly predicts the form of all the minimal energy solitons, even though it is a very simple model that includes only naive pair interactions.

A great advantage of the particle model is that it is computationally inexpensive to compute critical points of the binding energy, in comparison to more costly field theory simulations. In particular, this allows a large number of simulations to be performed to provide a measure of the capture basin for each critical point, and hence an estimate of the likelihood of finding the associated soliton solution in field theory computations, where the number of simulations that can be performed with reasonable resources is quite low. The frequency percentage shown in the last column of Table 2 provides the percentage of the 1000 computations in the particle model that produced the given critical point of δ. This data reveals that there are several examples where the optimal configuration is not the one that is obtained most often. This already occurs at the low value of $N = 4$, where more than three-quarters of the simulations produced the linear chain, rather than the optimal square arrangement.

In typical multi-dimensional soliton investigations, it is not practical to perform more than a handful of simulations for a given soliton number. In aloof soliton systems it therefore appears quite likely that global minimal energy solitons may be missed without the benefit of a reliable point particle model. This situation is highlighted by the $N = 9$ example, where the optimal 3×3 square arrangement was not obtained from any of six field theory simulations with random soliton initial conditions (this explains the earlier comment that most, rather than all, of the soliton solutions were obtained from randomly placed initial solitons). Given the particle model results this is not surprising, as this optimal $N = 9$ configuration was

obtained from only 8.2% of the 1000 random starting configurations. There is therefore a danger that, in aloof theories, soliton simulations alone may easily miss the optimal solution as capture basins can be relatively small.

5 A soliton lattice

The results presented so far with $N \leq 12$ reveal that hexagonal and square constituents are the prevalent sub-structures. This suggests that the optimal lattice (a doubly periodic configuration) will consist of either a hexagonal or a square arrangement. An indication that a hexagonal arrangement is more favourable than a square one is provided by the $N = 16$ case.

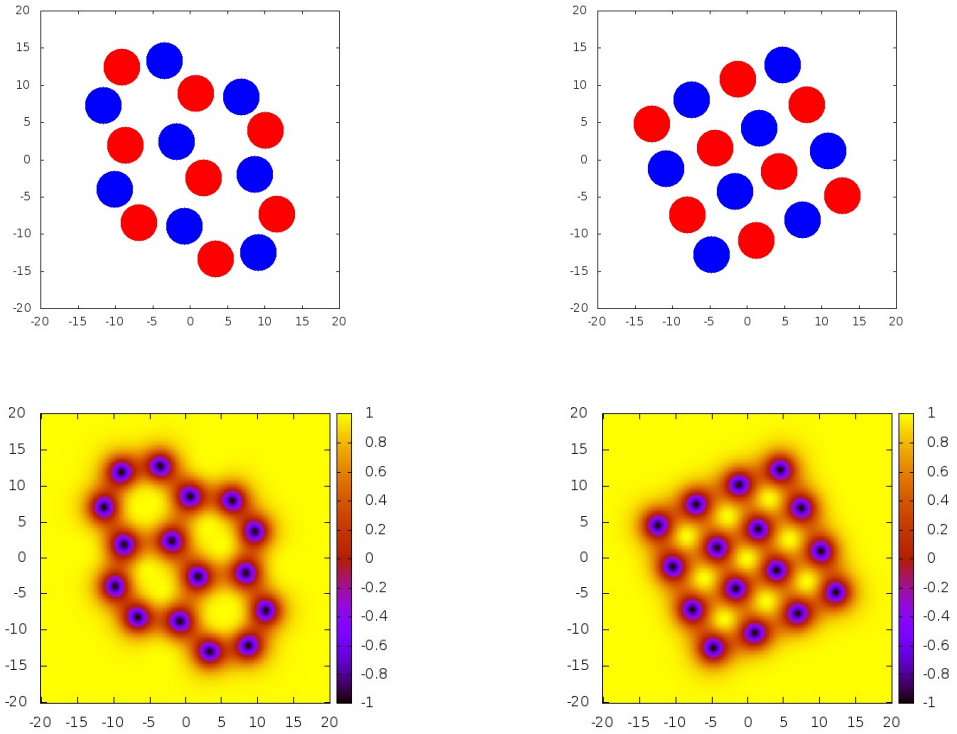

Figure 7: $N = 16$ critical points with hexagonal and square constituents. The top row is the particle model and the bottom row displays ϕ_3 for the field theory soliton solutions.

The global maximum of the binding energy for 16 particles is the hexagonal arrangement displayed in the top left image of Figure 7. This configuration has binding energy $\delta = 9.262$ and was obtained in 9.8% of 1000 random starts. The square configuration presented in the top right image of Figure 7 has a lower binding energy $\delta = 9.184$ (it is not even the next best configuration after the hexagonal solution) and was obtained in 6.8% of the simulations. Using the particle solutions to generate initial conditions for field theory simulations generates the associated soliton solutions shown in the bottom row of Figure 7. The soliton

solutions confirm the energy ordering of the particle model, with soliton binding energies of $\Delta = 9.437$ and $\Delta = 9.350$ for the hexagonal and square solutions respectively.

Guided by the hexagonal 16-soliton, we compute a doubly periodic hexagonal lattice containing four solitons on a fundamental cell $(x_1, x_2) \in [-L/2, L/2] \times [-L/(2\sqrt{3}), L/(2\sqrt{3})]$ with periodic boundary conditions. The maximal binding energy per soliton is $\Delta/N = 0.678$, obtained when $L = 18.03$, at which the area per soliton is $L^2/(4\sqrt{3}) = 46.9$. This soliton lattice is displayed in the left image in Figure 8, where we show two fundamental cells so that the hexagonal structure is clearly visible. The binding energy per soliton for this lattice is marked by the blue line in Figure 5 and is consistent with an asymptotic limit for the finite N solutions computed earlier. For large N a candidate for the optimal N-soliton solution is therefore an appropriate finite portion of this soliton lattice.

The square lattice with a fundamental cell $(x_1, x_2) \in [-L/2, L/2] \times [-L/2, L/2]$ containing four solitons has a maximal binding energy per soliton of $\Delta/N = 0.667$, obtained when $L = 13.15$ with the area per soliton equal to $L^2/4 = 43.2$. This confirms that the hexagonal lattice is energetically preferred over the square lattice. The right image in Figure 8 displays a fundamental cell for the square lattice. The binding energy per soliton for this lattice is marked by the red line in Figure 5.

We have verified that the conditions presented in [13], required for a doubly periodic solution to be a critical point with respect to variations of the lattice, are satisfied to a reasonable numerical accuracy. Indeed, symmetry arguments and the results in [14] show that both these lattice solutions are not only critical points with respect to variations of the lattice but are also stable.

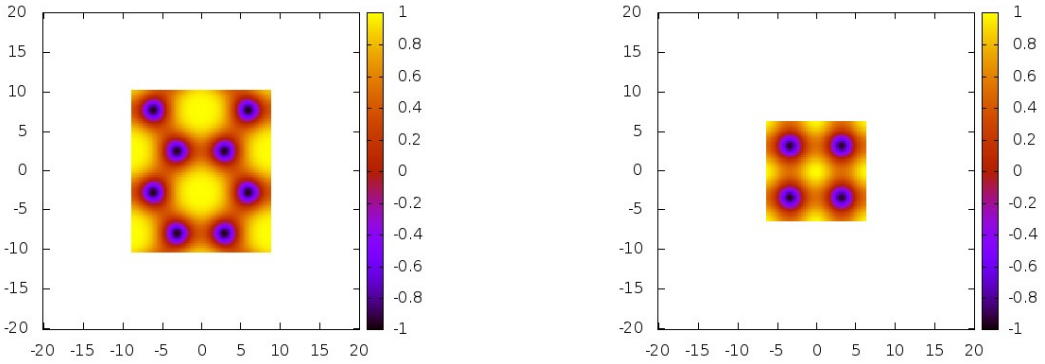

Figure 8: Plots of ϕ_3 in a periodic cell for the hexagonal lattice (left image) and the square lattice (right image).

6 Conclusion

Soliton binding energies in the standard Skyrme model are an order of magnitude larger than the nuclear binding energies that the model aims to reproduce. Furthermore, the solitons are often too symmetric, due to increased symmetries as individual solitons merge to form the bound state solutions. The symmetry of the soliton is important as it relates directly to the allowed quantum states via a collective coordinate quantization [15]. For example, the minimal energy 7-soliton has icosahedral symmetry [16] with a lowest allowed spin state $J = \frac{7}{2}$ [17], which disagrees with the ground state of ^{7}Li with spin $J = \frac{3}{2}$.

A Skyrme model in which single solitons retain their individual identities in bound states has the potential to resolve both the binding energy and symmetry issues. Here we have demonstrated that the required qualitative features can be obtained in a toy two-dimensional baby Skyrme model, based on perturbing a repulsive limit of the model. This provides further motivation for current work in progress [7] on the three-dimensional version of this problem.

We have demonstrated the utility of a binary species point particle approximation. The binary species aspect arises because all solitons can be assumed to have one of two possible internal phases. An alternative point particle approach could involve a single species with an arbitrary internal phase, but this generates the additional complication of computing the inter-particle force as a function of the relative internal phase. The results of the binary species model justify the use of this approximation and renders the extra complexity unnecessary. In a three-dimensional Skyrme model the internal phase is replaced by an internal $SO(3)$ isospin orientation, so the point particle model is a little more complicated. It remains to be seen whether a single species model, with each particle carrying an $SO(3)$ internal phase, or a multi-species model is more appropriate in this situation.

Acknowledgements

We thank Mike Gillard, Derek Harland and Martin Speight for useful discussions and a preview of their work in progress [7]. Our work is funded by the EPSRC grant EP/K003453/1 and the STFC grant ST/J000426/1.

References

[1] R.A. Battye and P.M. Sutcliffe, Skyrmions, fullerenes and rational maps, *Rev. Math. Phys.* **14**, 29 (2002).

[2] R.A. Battye, N.S. Manton and P.M. Sutcliffe, Skyrmions and the alpha-particle model of nuclei, *Proc. R. Soc.* **A463**, 261 (2007).

[3] C. Adam, J. Sanchez-Guillen and A. Wereszczynski, A Skyrme-type proposal for baryonic matter, *Phys. Lett.* **B691**, 105 (2010).

[4] C. Adam, C. Naya, J. Sanchez-Guillen and A. Wereszczynski, BPS Skyrme model and nuclear binding energies, *Phys. Rev. Lett.* **111**, 232501 (2013).

[5] P.M. Sutcliffe, Skyrmions, instantons and holography, *JHEP* **1008**, 019 (2010); Skyrmions in a truncated BPS theory, *JHEP* **1104**, 045 (2011).

[6] D. Harland, Topological energy bounds for the Skyrme and Faddeev models with massive pions, *Phys. Lett.* **B728**, 518 (2014).

[7] M. Gillard, D. Harland and J.M. Speight, in preparation.

[8] B.M.A.G. Piette, B.J. Schroers and W.J. Zakrzewski, Multisolitons in a two-dimensional Skyrme model, *Z. Phys.* **C65**, 165 (1995).

[9] R.A. Leese, M. Peyrard and W.J. Zakrzewski, Soliton scatterings in some relativistic models in (2+1) dimensions, *Nonlinearity* **3**, 773 (1990).

[10] G.S. Adkins and C.R. Nappi, The Skyrme model with pion masses, *Nucl. Phys.* **B233**, 109 (1984).

[11] D. Foster, Baby Skyrmion chains, *Nonlinearity* **23**, 465 (2010).

[12] J.M. Izquierdo, M.S. Rashid, B. Piette, and W.J. Zakrzewski, Models with solitons in (2+1) dimensions, *Z. Phys.* **C53**, 177 (1992).

[13] J. Jäykkä, J.M. Speight and P.M. Sutcliffe, Broken baby Skyrmions, *Proc. R. Soc.* **A468**, 1085 (2012).

[14] J.M. Speight, Solitons on tori and soliton crystals, *Commun. Math. Phys.* **332**, 355 (2014).

[15] D. Finkelstein and J. Rubinstein, Connection between spin, statistics and kinks, *J. Math. Phys.* **9**, 1762 (1968).

[16] R.A. Battye and P.M. Sutcliffe, Symmetric Skyrmions, *Phys. Rev. Lett.* **79**, 363 (1997).

[17] S. Krusch, Homotopy of rational maps and the quantization of Skyrmions, *Ann. Phys.* **304**, 103 (2003).

Configuration	Δ	δ	%
(i) 2*	0.701	0.698	100.0
(ii) 3*	1.272	1.153	100.0
(iii) 4*	1.884	1.740	21.7
(iv) 4	1.868	1.733	78.3
(v) 5*	2.457	2.260	93.9
(vi) 5	2.367	2.174	6.1
(vii) 6*	3.259	3.036	79.0
(viii) 6	3.042	2.820	11.2
(ix) 6	2.982	2.788	9.8
(x) 7*	3.651	3.407	73.6
(xi) 7	3.620	3.362	19.6
(xii) 7	3.564	3.310	4.4
(xiii) 7	3.406	3.264	2.4
(xiv) 8*	4.522	4.278	93.1
(xv) 8	4.281	4.060	1.0
(xvi) 8	4.100	3.916	0.4
(xvii) 8	4.053	3.837	5.5
(xviii) 9*	4.958	4.656	8.2
(xix) 9	4.906	4.632	82.0
(xx) 9	4.877	4.629	8.4
(xxi) 9	4.684	4.462	1.4
(xxii) 10*	5.750	5.466	85.2
(xxiii) 10	5.450	5.199	14.8
(xxiv) 11*	6.297	6.016	93.2
(xxv) 11	6.056	5.784	1.2
(xxvi) 11	5.934	5.707	3.0
(xxvii) 11	5.926	5.683	0.7
(xxviii) 11	5.705	5.499	1.9
(xxix) 12*	6.962	6.684	29.7
(xxx) 12	6.846	6.598	24.3
(xxxi) 12	6.827	6.589	0.2
(xxxii) 12	6.810	6.575	45.4
(xxxiii) 12	6.738	6.507	0.2
(xxxiv) 12	6.514	6.324	0.2

Table 2: Binding energies for N-solitons and binary species particles (with frequency %). * denotes the global maximum of the binding energy for each value of N.